ESC European Society of Cardiology

European Heart Journal - Cardiovascular Imaging (2019) **0**, 1–13
doi:10.1093/ehjci/jez185

Plaque burden can be assessed using intravascular optical coherence tomography and a dedicated automated processing algorithm: a comparison study with intravascular ultrasound

Edouard Gerbaud[1,2,3], Giora Weisz[4,5,6], Atsushi Tanaka[1,7], Romain Luu[1,8], Hany Ahmed Salaheldin Hussein Osman[1], Grace Baldwin[1], Pierre Coste[2,3], Laurent Cognet[8], Sergio Waxman[9], Hui Zheng[10], Jeffrey W. Moses[4,5], Gary S. Mintz[4,5], Takashi Akasaka[7], Akiko Maehara[4,5†], and Guillermo J. Tearney [1,11,12*†]

[1]Wellman Center for Photomedicine, Harvard Medical School and Massachusetts General Hospital, 40 Blossom Street, BHX-604A, Boston, MA 02114, USA; [2]Cardiology Intensive Care Unit and Interventional Cardiology, Hôpital Cardiologique du Haut Lévêque, 5 Avenue Magellan, Pessac 33600, France; [3]Bordeaux Cardio-Thoracic Research Centre, Bordeaux University, U1045, Hôpital Xavier Arnozan, Avenue du Haut Lévêque, Pessac 33600, France; [4]Columbia University Medical Center, New York, NY, USA; [5]Cardiovascular Research Foundation, 1700 Broadway, 9th Floor, New York, NY 10019, USA; [6]Montefiore-Einstein Center for Heart and Vascular, The University Hospital for the Albert Einstein College of Medicine, 111 East 210th Street, Bronx, NY 10467, USA; [7]Department of Cardiovascular Medicine, Wakayama Medical University, 811-1 Kimiidera, Wakayama, Wakayama Prefecture 641-8509, Japan; [8]Institut d'Optique Graduate School, CNRS—UMR 5298, Bordeaux University, Rue François Miterrand, Talence 33400, France; [9]Department of Cardiology, Lahey Clinic Medical Center, 41 Mall Road, Burlington, MA 01805, USA; [10]Biostatistics Center, Massachusetts General Hospital and Harvard Medical School, Boston, MA, USA; [11]Department of Pathology, Massachusetts General Hospital and Harvard Medical School, 40 Blossom Street, Boston, MA 02114, USA; and [12]Harvard-MIT Health Sciences and Technology, Boston, MA, USA

Received 7 April 2019; editorial decision 15 June 2019; accepted 10 July 2019

Aims Plaque burden (PB) measurement using intravascular optical coherence tomography (IVOCT) is currently thought to be inferior to intravascular ultrasound (IVUS). We developed an automated IVOCT image processing algorithm to enhance the external elastic lamina (EEL) contour. Thus, we investigated the accuracies of standard IVOCT and an IVOCT enhancement algorithm for measuring PB using IVUS as the reference standard.

Methods and results The EEL-enhancement algorithm combined adaptive attenuation compensation, exponentiation, angular registration, and image averaging using three sequential frames. In two different laboratories with intravascular imaging expertise, PB was quantified on 200 randomized, matched IVOCT and IVUS images by four independent observers. Fibroatheroma, fibrocalcific plaque, fibrous plaque, pathological intimal thickening (PIT), and mixed plaque were included in each set. Pearson's correlation coefficients between IVUS and standard IVOCT measurements of PB were 0.61, 0.67, 0.76, 0.78, and 0.87 for fibroatheromas, mixed plaques, fibrocalcific plaques, fibrous plaques, and PIT plaques, respectively. Pearson's correlation coefficients increased to 0.81, 0.83, 0.83, 0.84, and 0.90 when using the EEL-enhanced images ($P = 0.003$, $P = 0.004$, $P = 0.08$, $P = 0.12$, and $P = 0.23$, respectively). EEL-enhanced IVOCT analysis was associated with a lower EEL-area measurement absolute error for fibroatheromas, mixed plaques, and all pooled plaques ($P = 0.006$, $P = 0.02$, and $P < 0.001$, respectively). Compared with standard IVOCT, the EEL-enhanced IVOCT images had a higher sensitivity (79% vs. 28%, $P < 0.001$) and specificity (98% vs. 85%, $P = 0.03$) for plaques with an IVUS PB ≥70%.

* Corresponding author. Tel: +1 (617) 724 2979; Fax: +1 (617) 726 4103. E-mail: gtearney@partners.org

† The last two authors share senior authorship.

Conclusion EEL-enhanced IVOCT can be used to reliably measure PB in all types of coronary atherosclerotic lesions, including fibroatheromas and mixed plaques.

Keywords plaque burden • optical coherence tomography • intravascular ultrasound • algorithm

Introduction

Coronary atheroma progression including positive remodelling is linked to future clinical events such as acute coronary syndrome and sudden cardiac death.[1–3] The extent of atherosclerotic plaque is often quantified as plaque burden (PB), which is the percentage of plaque area within the entire vessel area. The largest prospective intravascular imaging atherosclerosis natural history study (PROSPECT) using intravascular ultrasound (IVUS) found that a PB ≥70% was an independent predictor of major adverse coronary events at 3-year follow-up.[4] IVUS and intravascular optical coherence tomography (IVOCT) are high-resolution imaging techniques that are increasingly being utilized in interventional cardiology for the investigation and management of coronary artery disease.[5,6] Although the resolution of IVOCT is 10 times superior to that of IVUS, the IVOCT technique is limited by attenuation of the backscattering signal in tissue.[7] The limited depth of penetration of IVOCT light at the atherosclerotic lesion site results in the loss of external elastic lamina (EEL) visibility in many lesions with large PB.[8] Key plaque features such as lipid, for example, manifest as a low IVOCT signal; and frequently the EEL is not readily visualized in these lesions. With the EEL contour of the diseased vessel not clearly visible, errors or difficulties in measuring PB are possible.[9,10] To mitigate this issue, some investigators have used plaque free wall[11] or lipid arc measurements as a surrogate marker of PB.[12]

A recent study by Teo *et al.*,[13] used attenuated-compensated IVOCT to show a significant improvement in EEL visualization in comparison to histology. Here, we developed an EEL enhancement algorithm that incorporates an attenuation compensation step.[13–15] To validate this new algorithm, we tested whether PB measurements using enhanced IVOCT images are superior to those obtained with conventional IVOCT images, by using measurements of PB from matched IVUS images as the reference standard.

Methods

Study population

Forty-two non-consecutive patients scheduled for elective percutaneous coronary intervention (PCI) were enrolled at two centres [Columbia University Medical Center (CUMC), New York, NY, USA and Lahey Clinic Medical Center, Burlington, MA, USA]. Massachusetts General Hospital (MGH-2005P000646), CUMC (Columbia IRB-AAAC3289), and Lahey IRBs (Lahey IC-ID 2005-46) approved the study protocol. The study complied with the Declaration of Helsinki and informed consent was obtained from all patients. Patients presenting with ST-elevation myocardial infarction, haemodynamic instability, renal insufficiency (glomerular filtration rate <50 mL/min), allergy to X-ray contrast, unprotected left main coronary artery disease, venous bypass graft lesions, chronic total occlusions, last remaining vessel, or extremely tortuous vessels were excluded. Supplementary data online, *Table S1* depicts baseline characteristics of the enrolled patients. Patients underwent the following procedures in the catheterization laboratory: coronary angiography, PCI of the culprit lesion, and intravascular imaging (IVUS and IVOCT imaging; Supplementary Materials) in random order.

Matched IVUS-IVOCT images sets

The matched IVUS-IVOCT images database was made by two independent interventional cardiologists (A.M. and A.T.) (Supplementary Materials). Among this initial database, images including stent struts or a lumen diameter >4.5 mm were excluded for this study. Five hundred and fifty matched IVUS-IVOCT images were obtained. Then, each IVOCT image was classified using standard IVOCT image interpretation criteria.[6,16] Tissue type for each frame was categorized as: fibroatheroma, fibrous plaque, fibrocalcific plaque, mixed plaque, and pathological intimal thickening (PIT). This plaque type classification was done by an expert IVOCT image reader in 550 IVOCT frames (E.G.) using IVOCT criteria.[6,16] Lipid plaque was identified as a signal-poor region with diffuse borders and an overlying signal-rich layer.[6] Fibrous plaque was defined as a lesion with homogeneous IVOCT signal and high backscattering.[6] Fibrocalcific plaque contained IVOCT evidence of fibrous tissue (defined previously) and calcium plates that appeared as signal-poor or heterogeneous regions with sharply delineated borders.[6] IVOCT heterogeneous lesions including fibroatheroma and calcific tissue were classified as mixed plaques.[17] PIT was defined as lesion that had intimal thickness ≥0.30 mm without clear evidence of lipid plaque. We defined intima thickness of ≥0.30 mm as pathological on the basis of histological studies of coronary arteries in young adults.[18] Sets of 200 IVUS-IVOCT matched images including fibrotheromas ($n = 40$), fibrous plaques ($n = 40$), fibrocalcific plaques ($n = 40$), mixed plaques ($n = 40$), and PITs ($n = 40$) were randomly selected from the 550 matched IVUS-IVOCT images by an independent researcher (R.L.) using randomization software on the website https://www.randomizer.org/.

Plaque burden processing algorithm

We created a dedicated optical coherence tomography (OCT) image processing algorithm to better delineate EEL on the IVOCT images, implemented using ImageJ software.[19] The automated processing algorithm combined adaptive attenuation compensation,[13,15] registration, and image averaging of successive frames from IVOCT pullback datasets (*Figure 1*). For each target frame of the set, substacks of ±1 frame around the centre frame [frame of interest (FOI)] were extracted from the pullback data. Following removal of tick marks using a median filter and correction of z-offset,[6] image substacks were converted to polar coordinates. Registration was accomplished using a custom correlation-based technique, implemented in the spatial frequency domain. Following stack registration, we applied an attenuation compensation plus exponentiation algorithm as described by Girard *et al.* and Teo *et al.*[13,15] Images were then converted back to Cartesian coordinates. For measurements on the algorithm-modified data, the processed FOI was used for manual lumen segmentation and a frame averaged image ($n = 3$, centred around the FOI) was employed for manual segmentation of the EEL. All images were corrected for an IVOCT compensation refractive index

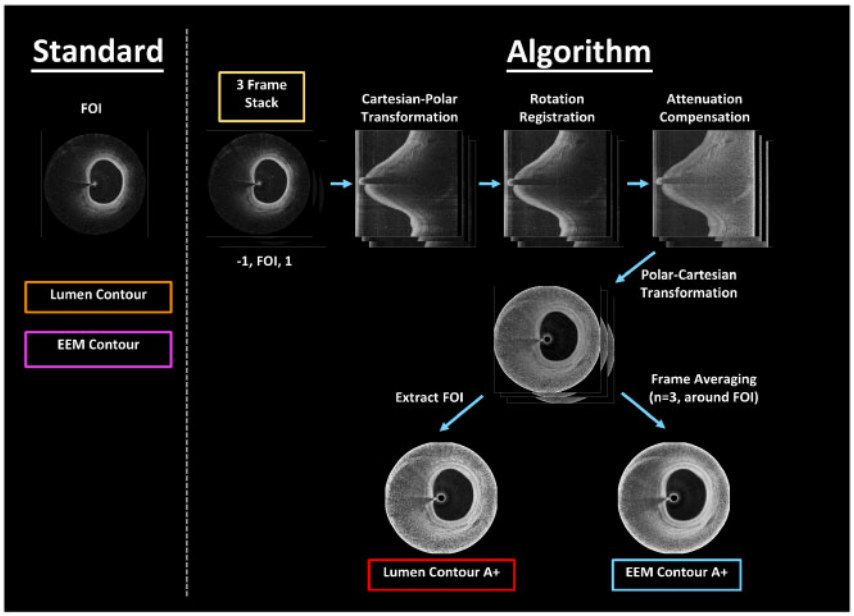

Figure 1 Schematic of the PB dedicated automated processing algorithm. For each target frame of the set, substacks of ±1 frame around the centre frame (frame of interest, FOI) were extracted from the pullback data. Following correction of z-offset, image substacks were converted to polar coordinates. Registration was accomplished using a correlation-based technique, implemented in the spatial frequency domain. Following stack registration, an attenuation compensation plus exponentiation algorithm was applied. Images were then converted back to Cartesian coordinates. For measurements on the algorithm-modified data, the processed FOI was used for manual lumen segmentation and a frame averaged image ($n = 3$, centred around the FOI) was employed for manual segmentation of the EEL.

of 1.4. Prior to segmentation, all images were brightness and contrast-balanced using ImageJ's integrated contrast normalization function.

IVUS vs. IVOCT data analysis

To assess quantitative PB measurements with and without the IVOCT EEL-enhancement algorithm vs. IVUS, randomized matched datasets of 200 IVOCT and 200 IVUS intracoronary images were analysed by four independent observers from two different laboratories (E.G and P.C. for the IVUS measurements; H.O and G.B for the IVOCT measurements) who were blinded to other data. Two expert IVUS readers (E.G and P.C.) manually delineated IVUS lumen and EEL contours. At the same time two non-expert IVOCT readers [H.O. (pathologist) and G.B. (technician)] manually delineated IVOCT lumen and EEL contours.

IVUS data analysis

IVUS measurements were made on a stand-alone computer workstation using ImageJ software. All quantitative data were evaluated following published consensus document definitions.[5] To evaluate the intra-observer variability, one observer (E.G.) repeated the analysis of another set after a one-month washout period.

IVOCT data analysis

Anonymized data were analysed on a stand-alone computer workstation using ImageJ software. The following quantitative data were measured: lumen cross-section area (CSA), EEL CSA, atheroma CSA, and PB. EEL and lumen borders were delineated following published consensus document definitions.[6,9] Observers quantified PB on all standard IVOCT images, even when the EEL was not completely identified on the entire circumference; where the EEL was not seen, the border where the IVOCT signal met noise was delineated (Supplementary data online, *Figure S1*). Similar measurements were then recorded using images processed by the EEL enhancement algorithm. Examples of the IVOCT images used in this study are shown in *Figures 2 and 3*. To evaluate the intra-observer variability, one observer (H.O.) repeated the measurements one month later.

Quantitative metrics

The following quantitative data were measured for standard and EEL-enhanced IVOCT and IVUS images: lumen CSA, EEL CSA, atheroma CSA (defined by the EEL CSA minus lumen CSA), PB [calculated as (atheroma CSA/EEL CSA) × 100 (%)].

Statistics

Continuous data are expressed as mean ± standard deviation, or median (interquartile range) when appropriate. Intra-observer and inter-observer variability for IVUS and IVOCT quantitative data were determined as mean (relative) difference (bias) and standard deviations according to the methods of Bland and Altman. The limits of agreement were defined as mean ± 1.96 standard deviation of the absolute difference. The relationships between the IVOCT and IVUS measurements were investigated using a linear regression analysis. A Pearson's correlation coefficient of 0.70 or higher indicates strong positive relationship; a r value of 0.50 to 0.69 indicates moderate positive relationship, and a r value of 0.30 to 0.49 indicates weak positive relationship. For comparisons within Pearson's correlation coefficients that are themselves inter-correlated, a z-test was performed according Eid *et al.* by using an online-calculator.[20] For comparisons within the magnitudes of

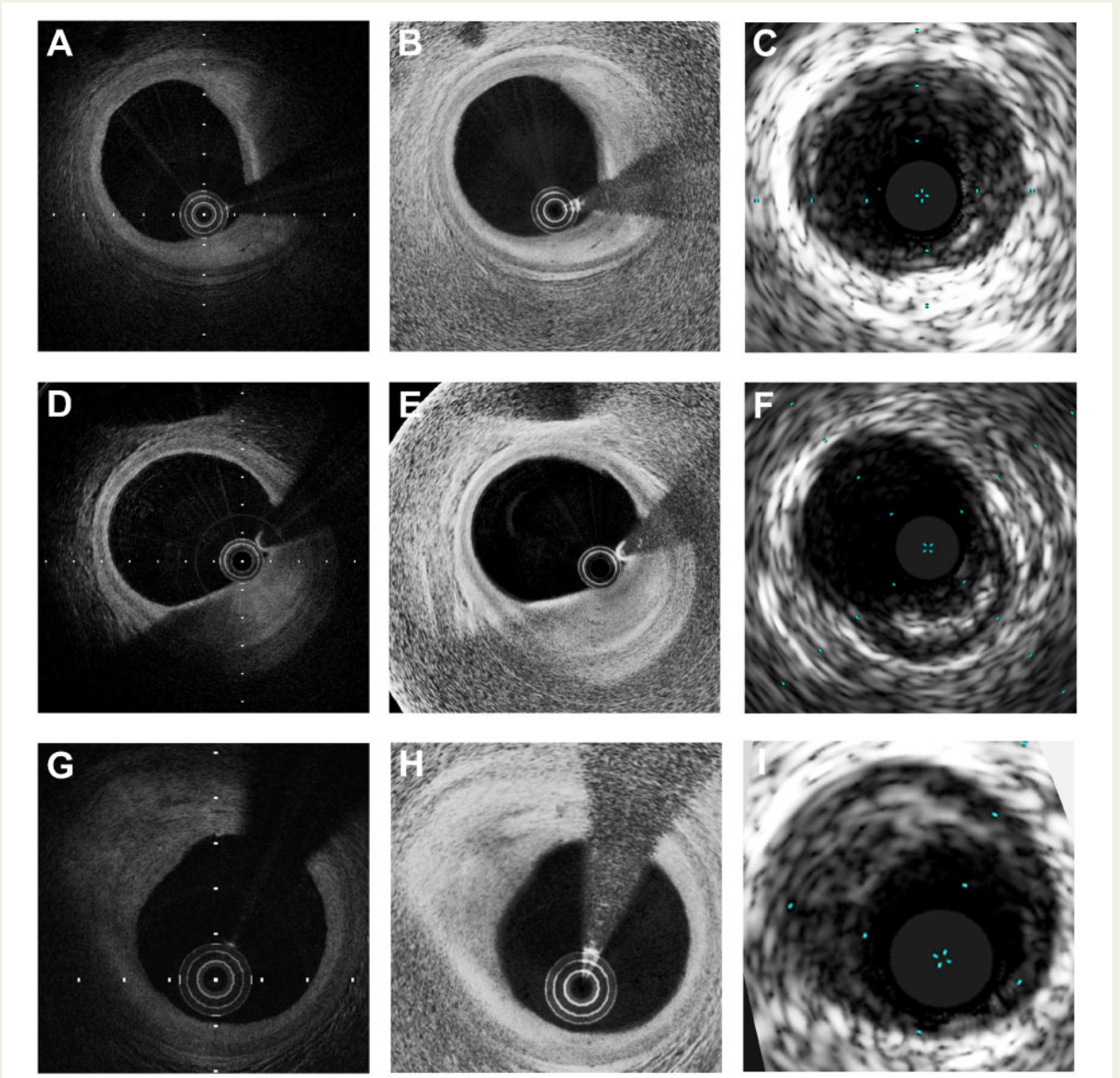

Figure 2 Examples of IVUS-IVOCT matched images with corresponding EEL-enhanced IVOCT images analysis using the dedicated PB algorithm. (*A*) IVOCT image of a fibroatheroma plaque. (*B*) Corresponding EEL-enhanced IVOCT image enabling improved visualization of the EEL deep to the plaque. (*C*) Corresponding IVUS image of this fibroatheroma plaque. (*D*) IVOCT image of another fibroatheroma plaque. (*E*) Corresponding EEL-enhanced IVOCT image enabling improved visualization of the EEL deep to the plaque. (*F*) Corresponding IVUS image of this fibroatheroma plaque. (*G*) IVOCT image of a mixed plaque. (*H*) Corresponding EEL-enhanced IVOCT image showing a more clearly delineated EEL. (*I*) Corresponding IVUS image of this mixed plaque.

intra-observer and inter-observer measurement differences of lumen CSA, EEL CSA, atheroma CSA, and PB between standard IVOCT and EEL-enhanced IVOCT images, a Wilcoxon signed rank test was performed. For comparisons within the absolute differences of EEL CSA measurements between IVUS and conventional IVOCT analyses vs. between IVUS and EEL-enhanced IVOCT analyses in each type of plaque and in all pooled plaques, a Wilcoxon signed rank test was also performed. Using IVUS PB = 70% as a cut-off value, standard IVOCT and EEL-enhanced IVOCT images sensitivity and specificity were calculated and statistically compared using a χ^2 test with a Yates' correction. *P*-values <0.05 were considered significant. All statistics were calculated using NCSS (NCSS 2001; NCSS Statistical software, Kaysville, Utah) and GraphPad Prism 7 (GraphPad Software, La Jolla, CA, USA), except for the comparison of correlations from dependent samples.

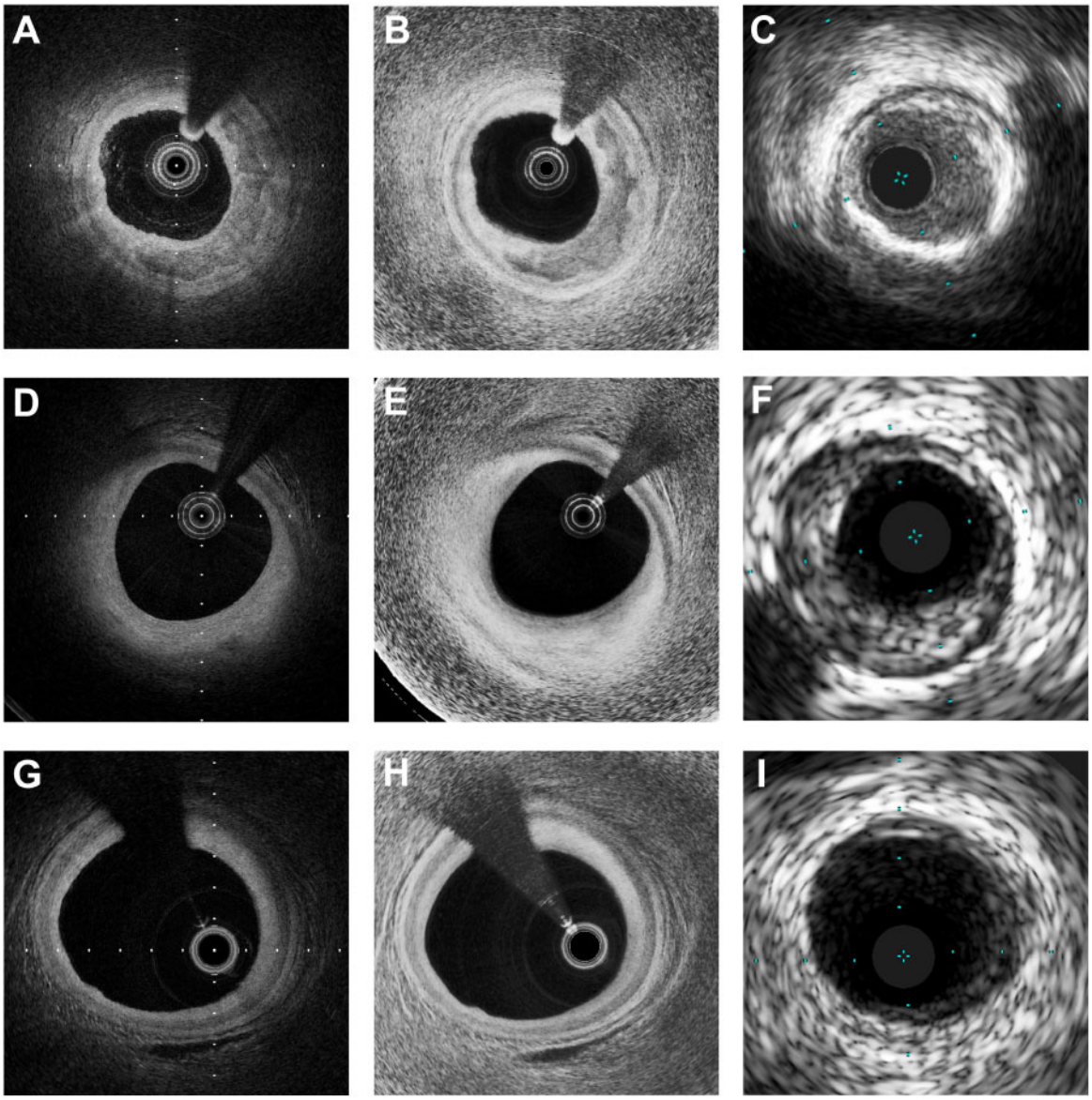

Figure 3 Examples of IVUS-IVOCT matched images with corresponding EEL-enhanced IVOCT images analysis using the dedicated PB algorithm. (*A*) IVOCT image of a fibrocalcific plaque. (*B*) Corresponding EEL-enhanced IVOCT showing a greatly improved capability to distinguish the EEL. (*C*) Corresponding IVUS image of this fibrocalcific plaque. (*D*) IVOCT image of a fibrous plaque. (*E*) Corresponding EEL-enhanced IVOCT showing much more of the EEL around the artery's circumference. (*F*) Corresponding IVUS image of this fibrous plaque. (*G*) IVOCT image of a pathological intimal thickening. (*H*) Corresponding EEL-enhanced IVOCT image. (*I*) Corresponding IVUS image of the pathological intimal thickening.

Results

Intra-observer and inter-observer variability for IVUS measurements

Intra-observer variability was very low for IVUS lumen CSA, EEL CSA, atheroma CSA, and PB measurements ($-0.05 \pm 0.27\ mm^2$, $0.16 \pm 0.82\ mm^2$, $-0.11 \pm 0.98\ mm^2$, $-0.06 \pm 3.1\%$, respectively). For inter-observer variability, the mean (standard deviation) differences were likewise low for IVUS lumen CSA, EEL CSA, atheroma CSA, and PB measurements ($-0.08 \pm 0.43\ mm^2$, $-0.13 \pm 1.09\ mm^2$, $-0.05 \pm 1.22\ mm^2$, $0.65 \pm 5.9\%$, respectively).

Intra-observer and inter-observer variability for standard IVOCT and EEL-enhanced IVOCT measurements

Intra-observer and inter-observer variability are shown in *Table 1*. The magnitude of intra- and inter-observer measurement differences for EEL-enhanced IVOCT was statistically significantly less than the

Table 1 Intra-observer and inter-observer variability for EEL-enhanced IVOCT vs. standard IVOCT PB measurements

	Mean difference IVOCT	Mean difference IVOCT + algorithm IVOCT A+	Absolute difference IVOCT	Absolute difference IVOCT + algorithm IVOCT A+	*P*-value
Intra-observer					
Lumen CSA (mm^2)	-0.05 ± 0.24	0.14 ± 0.12	0.11 (0.05–0.20)	0.09 (0.04–0.18)	0.17
EEL CSA (mm^2)	0.13 ± 1.62	0.12 ± 0.90	0.56 (0.23–1.36)	0.44 (0.16–0.92)	0.009
Atheroma CSA (mm^2)	-0.18 ± 1.61	-0.02 ± 0.89	0.54 (0.22–1.33)	0.42 (0.17–0.97)	0.009
Plaque burden (%)	0.97 ± 5.0	-0.65 ± 3.1	2.4 (1.2–5.0)	1.9 (0.8–3.2)	<0.001
Inter-observer					
Lumen CSA (mm^2)	0.02 ± 0.38	-0.09 ± 0.30	0.12 (0.05–0.25)	0.10 (0.05–0.17)	0.08
EEL CSA (mm^2)	-0.10 ± 2.27	-0.38 ± 1.03	0.79 (0.26–1.90)	0.60 (0.24–1.23)	<0.001
Atheroma CSA (mm^2)	-0.12 ± 2.24	-0.29 ± 1.04	0.80 (0.30–1.95)	0.60 (0.25–1.20)	<0.001
Plaque burden (%)	-1.22 ± 7.6	-0.63 ± 4.9	3.1 (1.3–6.5)	2.4 (0.9–4.4)	0.001

Values are expressed either as mean ± standard deviation or as median (interquartile range). Mean (relative) differences (bias) and standard deviations were calculated according to the methods of Bland and Altman.
Atheroma CSA was calculated as EEL CSA - lumen CSA. Plaque burden was calculated as (Atheroma CSA/EEL CSA) × 100 (%). *P*-value indicates the use of a Wilcoxon signed rank to compare IVOCT and EEL-enhanced IVOCT intra- and inter-observer mean differences magnitudes.
CSA, cross-section area; EEL, external elastic lamina; IVUS, intravascular ultrasound; IVOCT, intravascular optical coherence tomography; IVOCT A+, intravascular optical coherence tomography measurements using EEL-enhancement algorithm.

magnitude of intra- and inter-observer measurement differences for standard IVOCT for EEL CSA, atheroma CSA and PB.

Head-to-head comparison of IVUS and IVOCT measurements with and without automated EEL-enhancement algorithm

Fibroatheroma and mixed plaque

The median PB measurements by IVUS for fibroatheromas and mixed plaques were 63% (first quartile: 53%, third quartile: 75%, interquartile range: 22%) and 56% (first quartile: 46%, third quartile: 72%, interquartile range: 26%), respectively. PB ≥70% was measured by IVUS in 28 plaques (35%). The mean differences ± standard deviation of IVUS and IVOCT measurements with and without automated EEL-enhancement algorithm are presented in *Table 2*. The absolute value of the difference in EEL CSA measurements was reduced from 3.3 mm^2 (1.9–6.5) to 1.5 mm^2 (0.6–3.0) for fibroatheromas ($P = 0.006$), from 3.2 mm^2 (1.5–4.5) to 2.5 mm^2 (0.9–3.5) for mixed plaques ($P = 0.02$), when the automated EEL enhancement algorithm was used instead of standard IVOCT. Bland–Altman showed a moderate agreement for PB in fibroatheromas (5.0 ± 10.5%) and in mixed plaques (1.4 ± 11.4%) without the automated EEL-enhancement algorithm (*Figure 4*). Using the algorithm, the differences were lower for PB in fibroatheromas (1.7 ± 7.6%) and mixed plaques (2.4 ± 8.6%) (*Figure 5*). Without the automated EEL enhancement algorithm, Pearson's correlation coefficients between IVUS and standard IVOCT measurements for PB quantification were 0.61 and 0.67 for fibroatheromas and mixed plaques, respectively (*Table 3*). Using EEL-enhanced IVOCT images, Pearson's correlation coefficients increased to 0.81 and 0.83 for fibroatheromas and mixed plaques indicating a very strong positive relationship between IVUS and EEL-enhanced IVOCT PB quantification (*Figure 6*). The difference with vs. without the dedicated EEL enhancement algorithm for correlations between IVUS and IVOCT PB quantification was statistically significant for both types of plaque (fibroatheroma, $P = 0.003$; mixed plaque, $P = 0.004$). Using IVUS PB = 70% as a cut-off value, the EEL-enhanced IVOCT images also enabled a statistically significant improvement in sensitivity [79% (95% confidence interval (CI): 60–90) vs. 28% (95% CI: 15–47), $P < 0.001$] and specificity [98% (95% CI: 90–99) vs. 85% (95% CI: 76–93), $P = 0.03$] (*Table 4*).

Fibrocalcific plaque, mixed plaque, and pathological intimal thickening

The absolute value of the difference in EEL CSA measurements decreased not significantly from 2.8 mm^2 (0.9–4.7) to 2.4 mm^2 (1.1–3.7) for fibrocalcific plaques ($P = 0.44$), from 2.2 mm^2 (1.2–3.1) to 1.9 mm^2 (1.1–2.9) for fibrous plaques ($P = 0.40$), when EEL-enhanced IVOCT analysis was used instead of standard IVOCT analysis. Concerning PIT plaques, the absolute values of the difference in EEL CSA measurements with and without algorithm were quite similar: 0.4 mm^2 (0.2–0.7) vs 0.5 mm^2 (0.2–0.9), respectively ($P = 0.22$). Pearson's correlation coefficients values between IVUS and IVOCT measurements for PB were high in fibrocalcific plaques, in fibrous plaques and in PIT plaques (0.76, 0.78 and 0.87, respectively). In the same way, Pearson's correlation coefficients values between IVUS and EEL-enhanced IVOCT measurements for PB were high in fibrocalcific plaques, in fibrous plaques and in PIT plaques (0.83, 0.84, and 0.90, respectively) (*Figure 7*). The difference in Pearson's coefficients value between correlations with and without the automated EEL enhancement algorithm was not statistically significant in fibrocalcific plaques, in fibrous plaques and in PIT plaques ($P = 0.08$, $P = 0.12$, and $P = 0.23$, respectively).

All pooled plaques

The absolute value of the difference in EEL CSA measurements was reduced from 2.0 mm^2 (0.7–3.8) to 1.4 mm^2 (0.6–3.0) for all pooled plaques ($P < 0.001$), when EEL-enhanced IVOCT analysis was used

Table 2 Assessment of IVOCT measurements with and without algorithm in comparison with IVUS

	IVOCT	IVOCT + algorithm IVOCT A+	IVUS	Mean difference IVOCT vs. IVUS	Mean difference IVOCT A+ vs. IVUS
Fibroatheroma					
Lumen CSA (mm^2)	6.12 ± 3.74	6.23 ± 3.80	6.29 ± 3.59	0.16 ± 0.73	0.05 ± 0.91
EEL CSA (mm^2)	14.64 ± 8.35	15.83 ± 7.10	16.96 ± 6.28	2.33 ± 6.10	1.13 ± 4.64
Atheroma CSA (mm^2)	8.51 ± 5.36	9.44 ± 4.21	10.68 ± 4.39	2.16 ± 5.87	1.23 ± 4.33
Plaque burden (%)	58.6 ± 10.8	61.9 ± 12.0	63.6 ± 12.7	5.0 ± 10.5	1.7 ± 7.6
Mixed plaque					
Lumen CSA (mm^2)	5.85 ± 3.84	5.89 ± 3.84	6.07 ± 3.70	0.23 ± 0.65	0.19 ± 0.68
EEL CSA (mm^2)	12.70 ± 6.21	14.23 ± 7.32	14.33 ± 7.20	1.63 ± 4.34	0.10 ± 3.58
Atheroma CSA (mm^2)	6.85 ± 2.99	8.35 ± 4.54	8.25 ± 5.30	1.41 ± 4.21	-0.09 ± 3.31
Plaque burden (%)	55.4 ± 10.6	59.2 ± 11.5	56.8 ± 15.4	1.4 ± 11.4	-2.4 ± 8.6
Fibrocalcific plaque					
Lumen CSA (mm^2)	6.36 ± 3.26	6.43 ± 3.24	6.43 ± 3.13	0.07 ± 0.60	0.01 ± 0.57
EEL CSA (mm^2)	16.36 ± 5.04	16.87 ± 5.88	17.33 ± 4.80	0.96 ± 3.75	0.46 ± 3.62
Atheroma CSA (mm^2)	10.0 ± 3.05	10.44 ± 3.90	10.90 ± 2.89	0.90 ± 3.64	0.46 ± 3.44
Plaque burden (%)	62.3 ± 12.0	62.6 ± 11.7	63.9 ± 11.0	1.6 ± 7.9	1.3 ± 6.7
Fibrous plaque					
Lumen CSA (mm^2)	6.66 ± 2.96	6.82 ± 3.04	6.86 ± 2.77	0.20 ± 0.52	0.04 ± 0.48
EEL CSA (mm^2)	13.55 ± 4.32	14.20 ± 5.03	13.82 ± 3.75	0.27 ± 2.65	-0.38 ± 2.62
Atheroma CSA (mm^2)	6.89 ± 2.10	7.38 ± 2.49	6.97 ± 2.21	0.08 ± 2.43	-0.42 ± 2.31
Plaque burden (%)	52.4 ± 9.4	53.0 ± 8.8	51.1 ± 11.8	-1.1 ± 7.5	-1.9 ± 6.6
PIT					
Lumen CSA (mm^2)	7.76 ± 3.46	7.75 ± 3.30	7.91 ± 3.25	0.14 ± 0.51	0.16 ± 0.35
EEL CSA (mm^2)	10.81 ± 4.89	10.88 ± 4.83	10.95 ± 4.92	0.14 ± 0.80	0.07 ± 0.59
Atheroma CSA (mm^2)	3.05 ± 1.92	3.13 ± 2.12	3.04 ± 2.17	-0.01 ± 0.62	-0.09 ± 0.50
Plaque burden (%)	27.7 ± 8.5	27.7 ± 9.4	26.4 ± 8.2	-1.4 ± 4.2	-1.4 ± 4.1
All plaques					
Lumen CSA (mm^2)	6.57 ± 3.51	6.62 ± 3.48	6.71 ± 3.34	0.14 ± 0.60	0.09 ± 0.62
EEL CSA (mm^2)	13.62 ± 6.16	14.4 ± 6.39	14.68 ± 5.94	1.06 ± 3.99	0.27 ± 3.31
Atheroma CSA (mm^2)	7.05 ± 4.04	7.75 ± 4.36	7.97 ± 4.59	0.92 ± 3.83	0.22 ± 3.10
Plaque burden (%)	51.2 ± 16.1	52.9 ± 16.8	52.4 ± 18.3	1.1 ± 8.9	-0.5 ± 7.0

Values are expressed as mean ± standard deviation. Mean (relative) differences (bias) and standard deviations were calculated according to the methods of Bland and Altman. CSA, cross-section area; EEL, external elastic lamina; IVOCT, intravascular optical coherence tomography; IVOCT A+, intravascular optical coherence tomography measurements using EEL-enhancement algorithm; IVUS, intravascular ultrasound; PIT, pathological intimal thickening.

instead of standard IVOCT analysis. Pearson's correlation coefficients value between IVUS and IVOCT measurements for PB increased from 0.87 to 0.92, when EEL-enhanced IVOCT analysis was used instead of standard IVOCT analysis (Supplementary data online, *Figure S2*). The difference between these Pearson's correlation coefficients values was statistically significant ($P < 0.001$). Finally, as seen in the Bland–Altman plots in *Figure 5*, EEL-enhanced IVOCT measurements for PB have a negligible bias of ±1–2% with respect to IVUS.

Discussion

Our results show that for PIT, fibrous, and fibrocalcific plaque, standard IVOCT PB measurements closely approximate those of IVUS; however, the strong association breaks down for fibroatheromas and mixed plaques. EEL-enhanced IVOCT on the other hand was found to be satisfactory for measuring PB in all plaque types, including fibroatheromas and mixed plaques. This result is notable, as coronary atherosclerosis is frequently comprised of many different and potentially complex plaque morphologies. Importantly, the EEL-enhancement algorithm also significantly improved sensitivity/specificity of IVOCT for detecting lesions with PB ≥70%, using IVUS as the reference standard. This finding is significant as PB ≥70% is considered to be the single most predictive morphologic criterion for preemptively identifying the highest risk lesions in patients.[4,21]

Conventional wisdom is that EEL under the lipid-containing lesion is less well identified by IVOCT compared with IVUS.[10–12] Delineating EEL on IVOCT images is required to evaluate important features of coronary atherosclerosis such as PB and arterial remodelling. The IVOCT automated EEL-enhancement algorithm developed here combined several approaches including adaptive attenuation compensation, exponentiation for contrast enhancement. In the

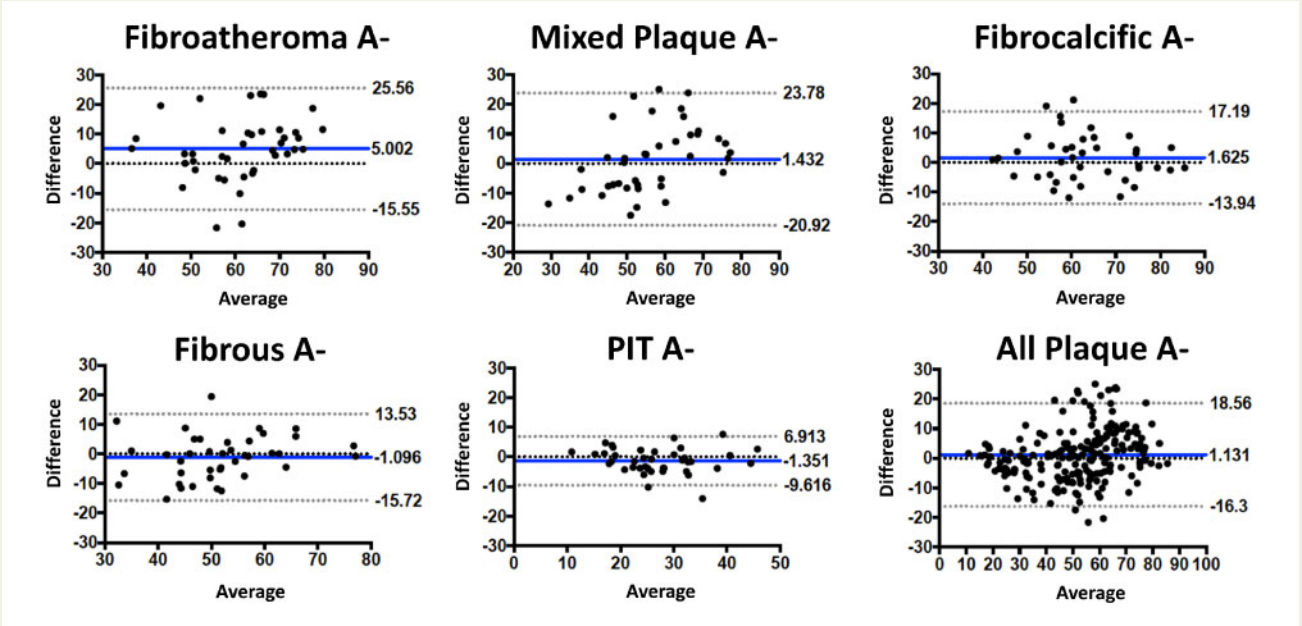

Figure 4 Bland–Altman analysis for measurements of standard IVOCT PB (%) in comparison with IVUS. Middle blue line: mean difference; top and bottom dotted lines: mean +1.96 SD and mean -1.96 SD, respectively.

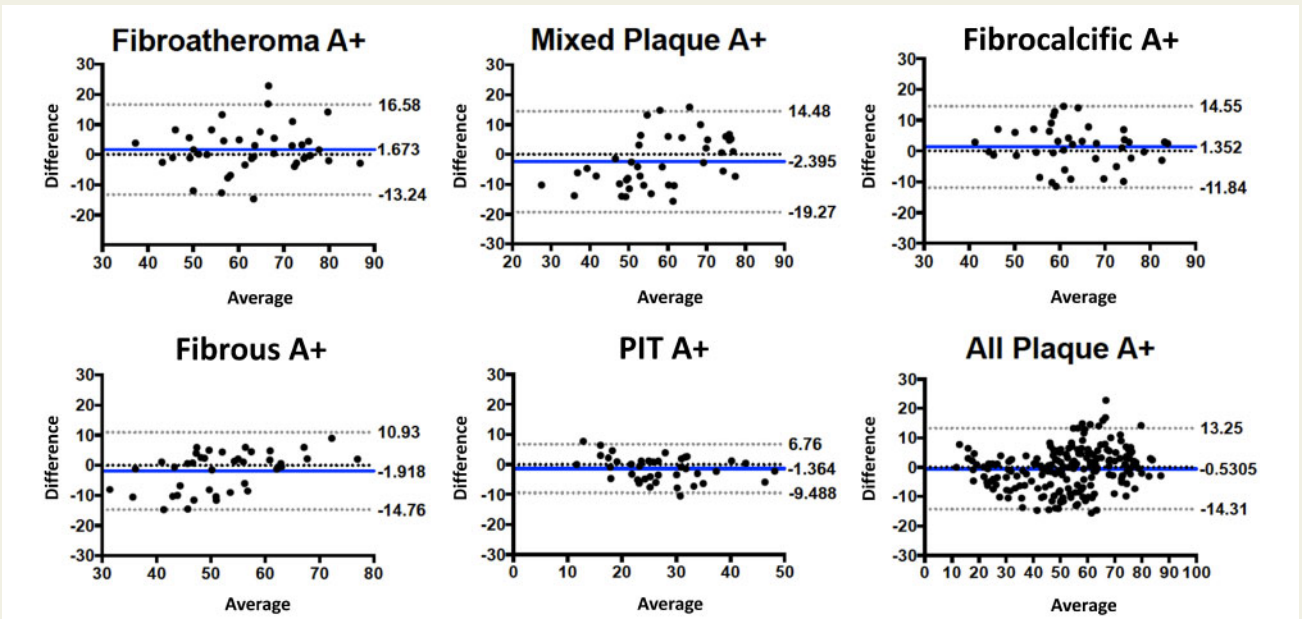

Figure 5 Bland–Altman analysis for measurements of EEL-enhanced IVOCT PB (%) in comparison with IVUS. Middle blue line: mean difference; top and bottom dotted lines: mean +1.96 SD and mean -1.96 SD, respectively.

human optic nerve head, Girard *et al.*[15] previously demonstrated that the combined use of compensation and exponentiation resulted in higher interlayer contrasts than those obtained with exponentiation only. In the same way, Teo *et al.* showed that this attenuation-compensated technique could be used on conventional IVOCT images and improve the detection of the EEL. However, this study was performed *ex vivo* and the EEL area was not quantified.[13] An additional component of our algorithm was the processing of 3D IVOCT data which included angular registration and image averaging using adjacent IVOCT frames. Thus, depth penetration enhancement was

Table 3 Assessment of IVOCT EEL CSA and PB (%) measurements with and without algorithm in comparison with IVUS

	Correlation		Linear regression			Bland–Altman	Limits of agreement[a]		Correlation		Linear regression			Bland–Altman	Limits of agreement[a]		Comparison of correlations[b]
	IVOCT vs. IVUS		IVOCT vs. IVUS			IVOCT vs. IVUS	IVOCT vs. IVUS		IVOCT A+ vs. IVUS		IVOCT A+ vs. IVUS			IVOCT A+ vs. IVUS	IVOCT A+ vs. IVUS		
	Pearson r	*P*-value	R^2	Equation of line	*P*-value	Bias, SD of bias	Lower	Upper	Pearson *r*	*P*-value	R^2	Equation of line	*P*-value	Bias, SD of bias	Lower	Upper	*P*-value
Fibroatheroma																	
EEL CSA (mm^2)	0.69	<0.0001	0.47	$Y = 9.42 + 0.52X$	<0.0001	2.33 ± 6.10	-9.6	14.3	0.77	<0.0001	0.59	$Y = 6.24 + 0.68X$	<0.0001	1.13 ± 4.64	-8.0	10.2	0.045
Plaque burden (%)	0.61	<0.0001	0.38	$Y = 21.53 + 0.72X$	<0.0001	5.0 ± 10.5	-15.6	25.6	0.81	<0.0001	0.66	$Y = 10.36 + 0.86X$	<0.0001	1.7 ± 7.6	-13.2	16.6	0.003
Mixed plaque																	
EEL CSA (mm^2)	0.69	<0.0001	0.47	$Y = 2.75 + 0.68X$	<0.0001	1.63 ± 4.34	-6.9	10.2	0.83	<0.0001	0.68	$Y = 1.61 + 0.86X$	<0.0001	0.10 ± 3.58	-6.9	7.1	0.01
Plaque burden (%)	0.67	<0.0001	0.45	$Y = 2.91 + 0.90X$	<0.0001	1.4 ± 11.4	-20.9	23.8	0.83	<0.0001	0.68	$Y = -9.13 + 1.11X$	<0.0001	-2.4 ± 8.6	-19.3	14.5	0.004
Fibrocalcific plaque																	
EEL CSA (mm^2)	0.71	<0.0001	0.51	$Y = 6.25 + 0.68X$	<0.0001	0.96 ± 3.75	-6.4	8.3	0.79	<0.0001	0.62	$Y = 6.47 + 0.65X$	<0.0001	0.46 ± 3.62	-6.6	7.6	0.047
Plaque burden (%)	0.76	<0.0001	0.58	$Y = 20.38 + 0.70X$	<0.0001	1.6 ± 7.9	-13.9	17.2	0.83	<0.0001	0.68	$Y = 15.55 + 0.77X$	<0.0001	1.3 ± 6.7	-11.8	14.6	0.08
Fibrous plaque																	
EEL CSA (mm^2)	0.79	<0.0001	0.63	$Y = 4.50 + 0.69X$	<0.0001	0.27 ± 2.65	-4.9	5.5	0.86	<0.0001	0.74	$Y = 4.70 + 0.65X$	<0.0001	-0.38 ± 2.62	-5.5	4.7	0.031
Plaque burden (%)	0.78	<0.0001	0.61	$Y = 3.57 + 0.91X$	<0.0001	-1.1 ± 7.5	-15.7	13.5	0.84	<0.0001	0.70	$Y = -8.96 + 1.13X$	<0.0001	-1.9 ± 6.6	-14.8	10.9	0.12
PIT																	
EEL CSA (mm^2)	0.99	<0.0001	0.97	$Y = 0.23 + 0.99X$	<0.0001	0.14 ± 0.80	-1.4	1.7	0.99	<0.0001	0.99	$Y = -0.06 + 1.01X$	<0.0001	0.07 ± 0.59	-1.1	1.2	0.014
Plaque burden (%)	0.87	<0.0001	0.76	$Y = 3.37 + 0.83X$	<0.0001	-1.4 ± 4.2	-9.6	6.9	0.90	<0.0001	0.81	$Y = 4.99 + 0.77X$	<0.0001	-1.4 ± 4.1	-9.5	6.8	0.23
All plaques																	
EEL CSA (mm^2)	0.78	<0.0001	0.61	$Y = 4.39 + 0.76X$	<0.0001	1.06 ± 3.99	-6.8	8.9	0.86	<0.0001	0.74	$Y = 3.18 + 0.81X$	<0.0001	0.27 ± 3.31	-6.2	6.8	<0.001
Plaque burden (%)	0.87	<0.0001	0.76	$Y = 1.41 + 0.99X$	<0.0001	1.1 ± 8.9	-16.3	18.6	0.92	<0.0001	0.85	$Y = -0.61 + 1.01X$	<0.0001	-0.5 ± 7.0	-14.3	13.2	<0.001

Pearson's correlation coefficients, linear regression analysis (including R^2, equation of line, and *P*-values), Bland–Altman analysis (including bias, SD of bias and limits of agreement) and comparisons within Pearson's correlation coefficients (correlation of standard IVOCT and IVUS measurements vs. correlation of EEL-enhanced IVOCT and IVUS measurements) are successively presented. Values are expressed as mean ± standard deviation (SD).

[a]Bland–Altman limits of agreement are defined as mean ± 1.96 SD of absolute difference.

[b]A *z*-test was performed to compare Pearson's correlation coefficients that are themselves inter-correlated. IVOCT A+ indicates intravascular optical coherence tomography measurements using the EEL-enhancement algorithm.

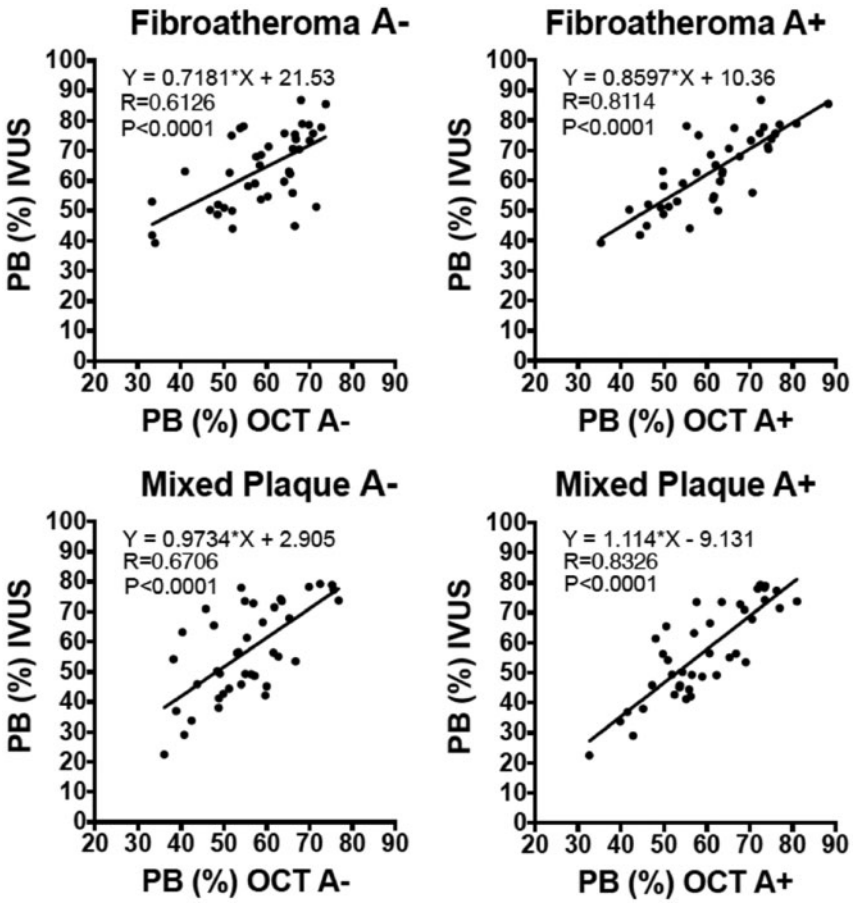

Figure 6 Assessment of IVOCT PB measurements in fibroatheromas and in mixed plaques with and without algorithm in comparison with IVUS. Regression analysis for measurements of PB percentages between standard IVOCT and IVUS (left panel), between EEL-enhanced IVOCT and IVUS (right panel), in case of fibroatheroma (upper panels), and mixed plaque (lower panels).

Table 4 Assessment of fibroatheroma and mixed plaques luminal narrowing with and without algorithm in comparison with IVUS

Fibroatheroma and mixed plaques characteristics ($n = 80$)	IVUS	Standard IVOCT	IVOCT A+
Number of cases with ≥70% luminal narrowing	28 (35)	16 (20)	23 (28)
Matched cases on IVUS and IVOCT measurements		8	22
Number of cases with <70% luminal narrowing	52 (65)	64 (80)	57 (72)
Matched cases on IVUS and IVOCT measurements		44	51

Values in parentheses are percentages.
IVOCT A+, intravascular optical coherence tomography measurements using EEL-enhancement algorithm; IVUS, intravascular ultrasound.

increased due the merging of three images centred on the slice of interest in order to pool similar characteristics of the different layers and constituents of the plaques.

There is an overwhelming perception that IVUS is the only intravascular imaging technique that is capable of accurately measuring PB *in vivo*. It is well-known that EEL delineation of IVOCT images is dependent on tissue type. Indeed, near-infrared light used by IVOCT is attenuated more rapidly by lipid than with fibrotic or fibrocalcific tissue.[7,22,23] This characteristic of IVOCT has motivated the development of IVOCT measurements that may be related to PB. Kubo *et al.*[12] for example developed an approximating algorithm for measuring vessel area in coronary arteries with lipid-rich plaque, compared with IVUS. They observed a good agreement between IVOCT and IVUS measured vessel areas (Pearson's correlation coefficient value of 0.834). However, the mean difference and limits of agreement increased with an increase in lipid arc in their study.

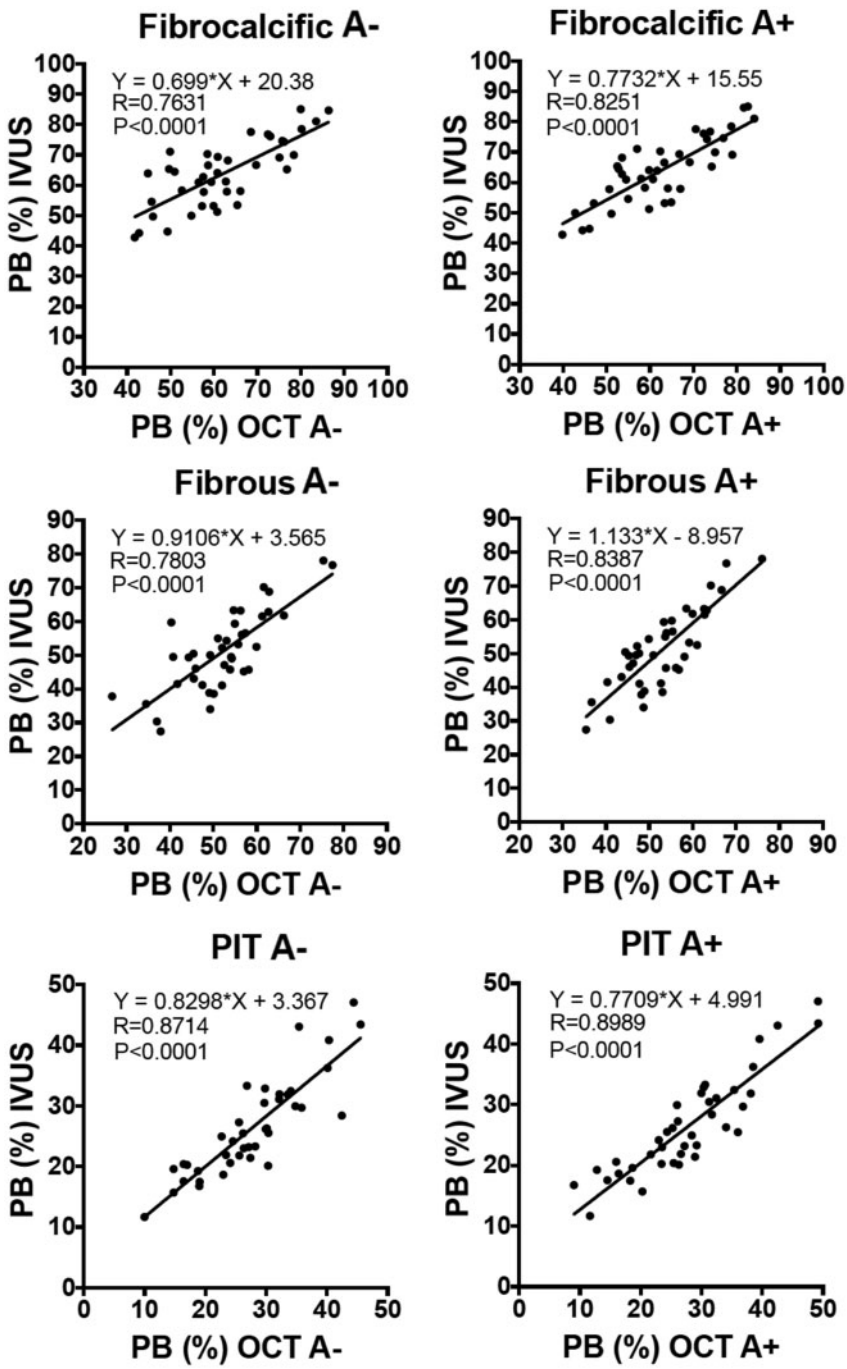

Figure 7 Assessment of IVOCT PB measurements in fibrocalcific plaques, in fibrous plaques, and in PIT plaques with and without algorithm in comparison with IVUS. Regression analysis for measurements of PB percentages between standard IVOCT and IVUS (left panel), between EEL-enhanced IVOCT and IVUS (right panel), in case of fibrocalcific plaque (upper panels), fibrous plaque (mid panels), and pathological intimal thickening (lower panels).

Furthermore, this approximating algorithm had some limitations; it could not be used in in oval or irregular vessels, for instance. The EEL-enhancement technique described here has no such limitations.

In our study, the additional value of a dedicated EEL-enhancement algorithm was predominant in fibroatheromas and in mixed plaques ($P = 0.003$ and $P = 0.004$, respectively). While the algorithm reported in this article greatly closes the gap between IVOCT and IVUS for CSA and PB measurements, atheroma CSA is still underestimated by IVOCT in fibroatheromas and less so in mixed plaque, possibly owing to residual penetration depth limitations of IVOCT. While EEL

enhancement may not be necessary for measuring PB in fibrocalcific plaques, caution must be taken in the analysis of the results because signal attenuation can occur with IVUS in areas of calcium.[24] IVOCT may in fact be superior to IVUS for measuring PB in fibrocalcific plaques as shown in Supplementary data online, *Figure S3*. This figure shows that IVOCT light penetrates calcium, enabling EEL visualization, whereas EEL visualization is difficult for IVUS due to the attenuation of ultrasound by calcium.

Previously, we showed that IVOCT approximates IVUS PB when the EEL is clearly delineated all around its circumference.[10] In the current study, the IVOCT automated EEL-enhancement algorithm helped to reliably visualize the EEL even when the EEL was not completely identified on the entire circumference. Interventional cardiologists using IVOCT are often faced with the limitation of the attenuation and difficulty to obtain good EEL-based measurements in order to choose stent diameters. Interestingly, an EEL-based OCT-guided PCI strategy has been proposed and tested in the prospective, multicentre randomized ILUMIEN III: OPTIMIZE PCI study.[25] Interventional cardiologists were able to delineate EEL >180° in the reference segments in 84% of cases (vs. 83% by IVUS), whereas in the core laboratory, the success rates were 95% and 100%, respectively. The use of the automated EEL-enhancement algorithm described here may facilitate EEL delineation for PCI guidance in the catheterization laboratory and for the broader interventional cardiologist community.

Study limitations

Our study included a small number of images ($n = 200$; 40 per set). However, the analysis was complete, including a wide range of different types of atherosclerotic plaques. To generate the sets, images with poor quality were excluded, which may have induced selection bias, although the investigators who excluded images did not participate in EEL measurement. As with all studies of this sort, the matching process may have had some imperfections. Furthermore, EEL visualization in echo-attenuated plaques by IVUS is sometimes difficult. Depending on the arc of the attenuated plaques, intra-observer and inter-observer variabilities of IVUS PB measurements may have been slightly impacted. This study was conducted in two highly experienced centres in intravascular imaging in the USA and in Europe. Thus, the results of this study may not be applicable elsewhere. Parameters like vascular tonus, vessel location, vessel with a lumen diameter > 4.5 mm, flushing media and variation of cardiac cycle that could affect differences between IVOCT and IVUS assessments were not incorporated in the analysis. Finally, further research is needed to determine whether this EEL enhancement algorithm can be translated into clinical use. Reproduction of this work in larger studies is therefore merited.

Conclusions

A dedicated automated processing algorithm can be applied to conventional IVOCT images in order to improve EEL contour delineation. EEL-enhanced IVOCT measurements of PB were strongly correlated to IVUS PB measurements for all plaque types, even in fibroatheromas and in mixed plaques. Using this algorithm, IVOCT can be used to reliably measure PB.

Supplementary data

Supplementary data are available at *European Heart Journal - Cardiovascular Imaging* online.

Acknowledgements

The authors would like to thank Mireille Rosenberg and Gabriela Apiou-Sbirlea for their assistance.

Funding

The work was supported by the National Institutes of Health (R01HL076398).

Conflict of interest: Massachusetts General Hospital has a patent licensing arrangement with Terumo Corporation. G.J.T. has the right to receive royalties as part of this licensing arrangement; also receives royalties from MIT and Nidek; has a financial/fiduciary interest in Spectrawave, a company developing an OCT-NIRS intracoronary imaging system and catheter; his financial/fiduciary interest was reviewed and is managed by the Massachusetts General Hospital and Partners HealthCare in accordance with their conflict of interest policies; receives catheter materials from Terumo; is a consultant for NinePoint and Spectrawave and receives sponsored research from Canon and Vivolight. A.K. is a consultant for Boston Scientific and received institutional grant from Abbott Vascular and Boston Scientific. G.W. sits on the advisory boards of Corindus, Filterlex, and Trisol. G.W. and Montefiore Medical Center have received institutional research grants from Abbott, Corindus, CSI, Renalguard, and Svelete. G.S.M. is a consultant for Boston Scientific, Volcano/Philips and Infraredx. E.G. is a consultant for Terumo. All other authors declared no conflict of interest.

References

1. Ambrose JA, Tannenbaum MA, Alexopoulos D, Hjemdahl-Monsen CE, Leavy J, Weiss M *et al.* Angiographic progression of coronary artery disease and the development of myocardial infarction. *J Am Coll Cardiol* 1988;**12**:56–62.
2. Azen SP, Mack WJ, Cashin-Hemphill L, LaBree L, Shircore AM, Selzer RH *et al.* Progression of coronary artery disease predicts clinical coronary events. Long-term follow-up from the Cholesterol Lowering Atherosclerosis Study. *Circulation* 1996;**93**:34–41.
3. Motoyama S, Ito H, Sarai M, Kondo T, Kawai H, Nagahara Y *et al.* Plaque characterization by coronary computed tomography angiography and the likelihood of acute coronary events in mid-term follow-up. *J Am Coll Cardiol* 2015;**66**:337–46.
4. Stone GW, Maehara A, Lansky AJ, de Bruyne B, Cristea E, Mintz GS *et al.* A prospective natural-history study of coronary atherosclerosis. *N Engl J Med* 2011;**364**:226–35.
5. Mintz GS, Nissen SE, Anderson WD, Bailey SR, Erbel R, Fitzgerald PJ *et al.* American College of Cardiology clinical expert consensus document on standards for acquisition, measurement and reporting on intravascular ultrasound studies (IVUS). A report of the American College of Cardiology task force on clinical expert consensus documents. *J Am Coll Cardiol* 2001;**37**:1478–92.
6. Tearney GJ, Regar E, Akasaka T, Adriaenssens T, Barlis P, Bezerra HG *et al.* Consensus standards for acquisition, measurement, and reporting of intravascular optical coherence tomography studies. *J Am Coll Cardiol* 2012;**59**:1058–72.
7. Xu C, Schmitt JM, Carlier SG, Virmani R. Characterization of atherosclerosis plaques by measuring both backscattering and attenuation coefficients in optical coherence tomography. *J Biomed Opt* 2008;**13**:034003.
8. Bezerra HG, Costa MA, Guagliumi G, Rollins AM, Simon DI. Intracoronary optical coherence tomography: a comprehensive review: clinical and research applications. *J Am Coll Cardiol Cardiovasc Interv* 2009;**2**:1035–46.
9. Prati F, Guagliumi G, Mintz GS, Costa M, Regar E, Akasaka T *et al.* Expert review document part 2: methodology, terminology and clinical applications of optical coherence tomography for the assessment of interventional procedures. *Eur Heart J* 2012;**33**:2513–20.
10. Gerbaud E, Weisz G, Tanaka A, Kashiwagi M, Shimizu T, Wang L *et al.* Multi-laboratory inter-institute reproducibility study of IVOCT and IVUS assessments using published consensus document definitions. *Eur Heart J Cardiovasc Imaging* 2016;**17**:756–64.
11. Hoogendoorn A, Gnanadesigan M, Zahnd G, van Ditzhuijzen NS, Schuurbiers JCH, van Soest G *et al.* OCT-measured plaque free wall angle is indicative for

plaque burden: overcoming the main limitation of OCT? *Int J Cardiovasc Imaging* 2016;**32**:1477–81.
12. Kubo T, Yamano T, Liu Y, Ino Y, Shiono Y, Orii M *et al*. Feasibility of optical coronary tomography in quantitative measurement of coronary arteries with lipid-rich plaque. *Circ J* 2015;**79**:600–6.
13. Teo JC, Foin N, Otsuka F, Bulluck H, Fam JM, Wong P *et al*. Optimization of coronary optical coherence tomography imaging using the attenuation compensated technique: a validation study. *Eur Heart J Cardiovasc Imaging* 2017;**18**:880–8.
14. Lee R, Foin N, Otsuka F, Wong P, Mari JM, Joner M *et al*. Intravascular assessment of arterial disease using compensated OCT in comparison with histology. *JACC Cardiovasc Imaging* 2016;**9**:321–2.
15. Girard MJA, Strouthidis NG, Ethier CR, Mari JM. Shadow removal and contrast enhancement in optical coherence tomography images of the human optic nerve head. *Invest Ophthalmol Vis Sci* 2011;**52**:7738–48.
16. Otsuka F, Joner M, Prati F, Virmani R, Narula J. Clinical classification of plaque morphology in coronary disease. *Nat Rev Cardiol* 2014;**11**:379–89.
17. Athanasiou LS, Exarchos TP, Naka KK, Michalis LK, Prati F, Fotiadis DI. Atherosclerotic plaque characterization in optical coherence tomography images. *Conf Proc IEEE Eng Med Biol Soc* 2011;**32**:4485–8.
18. Velican D, Velican C. Comparative study on age-related changes and atherosclerotic involvement of the coronary arteries of male and female subjects up to 40 years of age. *Atherosclerosis* 1981;**38**:39–50.
19. Schneider CA, Rasband WS, Eliceiri KW. NIH Image to ImageJ: 25 years of image analysis. *Nat Methods* 2012;**9**:671–5.
20. Lenhard W, Lenhard A. *Hypothesis Tests for Comparing Correlations*. 2014. https://www.psychometrica.de/correlation.html (15 March 2017, date last accessed).
21. Yun KH, Mintz GS, Farhat N, Marso SP, Taglieri N, Verheye S *et al*. Relation between angiographic lesion severity, vulnerable plaque morphology and future adverse cardiac events (from the Providing Regional Observations to Study Predictors of Events in the Coronary Tree study). *Am J Cardiol* 2012;**110**:471–7.
22. Kubo T, Tanaka A, Ino Y, Kitabata H, Shiono Y, Akasaka T. Assessment of coronary atherosclerosis by optical coherence tomography. *J Atheroscler Thromb* 2014;**21**:895–903.
23. Schmitt JM, Xiang SH, Yung KM. Speckle in optical coherence tomography. *J Biomed Opt* 1999;**4**:95–105.
24. Wang X, Matsumura A, Mintz GS, Lee T, Zhang W, Cao Y *et al*. *In vivo* calcium detection by comparing optical coherence tomography, intravascular ultrasound, and angiography. *JACC Cardiovasc Imaging* 2017;**10**:869–79.
25. Ali ZA, Maehara A, Genereux P, Shlofmitz RA, Fabbiocchi F, Nazif TM *et al*. Optical coherence tomography compared with intravascular ultrasound and with angiography to guide coronary stent implantation (ILUMIEN III: oPTIMIZE PCI): a randomised controlled trial. *Lancet* 2016;**388**:2618–28.